Ingeniería y Competitividad
Vol 27 (3) 2025 doi: 10.25100/iyc.v27i3.14715

Vol 27 (3)

ISSN
0123-3033
e- 2027-8284

Original Article

The effect of coating thickness on cavitation erosion of epoxy systems

El efecto del espesor del recubrimiento en la erosión por cavitación de los sistemas epóxicos

G.L. García[1] A. Espinosa[2] J.F. Santa[3]

[1] Computational Mechanical Design Group, Universidad Nacional de Colombia, Medellín, Colombia
[2] Software Quality Research Group, Universidad Nacional de Colombia, Medellín, Colombia
[3] Tribology and Surfaces Group, Universidad Nacional de Colombia, Medellín, Colombia

Abstract

Introduction: cavitation erosion is a common issue in hydraulic machines because it decreases their efficiency. Epoxy coatings are often applied to repair worn components and improve their durability.
Objectives: this work studies the cavitation erosion behavior of three multilayer epoxy coating systems with different thicknesses to evaluate their resistance and identify the most effective configuration.
Methodology: cavitation tests were conducted according to the ASTM G32 standard. A weak shock model was used to calculate the mechanical behavior of the coatings under cavitation wear, determining the maximum pressure values at the coating surface (Pmax). The wear marks produced by the impact of shock waves were analyzed by Scanning Electron Microscopy (SEM) to characterize the surface damage and wear mechanisms.
Results: the thinner coating, with a thickness of 380 µm, exhibited the longest incubation period of 271 seconds. In contrast, the thickest coating showed the highest erosion rate of 2822 mg/min. The calculated pressures from impact shock waves were significantly lower than the coating hardness (H), indicating that surface damage was not due to direct plastic deformation. SEM observations revealed the formation of crazing and crack coalescence during the incubation period, confirming that surface fatigue and microcrack propagation dominate the wear process.
Conclusions: the results demonstrate that coating thickness strongly influences cavitation resistance. Thinner coatings delay the onset of erosion, while thicker layers experience higher erosion rates due to accumulated internal stresses and crack propagation.

Keywords: Acoustic Cavitation, ASTM G32, Cavitation Damage, Epoxy Coating Systems, Fatigue; Shock Wave.

Resumen

Introducción: la erosión por cavitación es un problema común en las máquinas hidráulicas, ya que reduce su eficiencia. Los recubrimientos epóxicos se utilizan con frecuencia para reparar componentes desgastados y mejorar su durabilidad.
Objetivos: este trabajo estudia el comportamiento frente a la erosión por cavitación de tres sistemas de recubrimientos epóxicos multicapa con diferentes espesores, con el fin de evaluar su resistencia y determinar la configuración más efectiva.
Metodología: las pruebas de cavitación se realizaron conforme a la norma ASTM G32. Se utilizó un modelo de onda de choque débil para calcular el comportamiento mecánico de los recubrimientos sometidos a desgaste por cavitación, determinando los valores máximos de presión en la superficie (Pmax). Las huellas de desgaste producidas por el impacto de las ondas de choque se analizaron mediante microscopía electrónica de barrido (SEM) para caracterizar el daño superficial y los mecanismos de desgaste.
Resultados: el recubrimiento más delgado, con un espesor de 380 µm, presentó el período de incubación más largo, de 271 segundos. En cambio, el recubrimiento más grueso mostró la mayor tasa de erosión, de 2822 mg/min. Los valores de presión calculados fueron significativamente menores que la dureza del sistema de recubrimiento (H), indicando que el daño no se debió a deformación plástica directa. Las observaciones por SEM revelaron la formación de fisuras y la coalescencia de grietas durante el período de incubación.
Conclusiones: los resultados demuestran que el espesor del recubrimiento influye fuertemente en la resistencia a la cavitación: los recubrimientos delgados retrasan el inicio de la erosión, mientras que los más gruesos presentan mayores tasas de desgaste debido a tensiones internas acumuladas y propagación de grietas.

Palabras clave: Cavitación acústica, ASTM G32, daños por cavitación, sistemas de recubrimiento epóxico, fatiga; ondas de choque

How to cite?

García GL, Espinoza A, Santa JF. The effect of coating thickness on cavitation erosion of epoxy systems. Ingeniería y Competitividad, 2025, 27(3)e-20114715

https://doi.org/10.25100/iyc.v27i3.14715

Received: 28/01/25
Reviewed: 25/04/25
Accepted: 17/09/25
Online: 10/11/25

Correspondence

glgarcia@unal.edu.co

Spanish version

Why was this study conducted?
This work was done to evaluate the effect of coating thickness on cavitation erosion of epoxy systems. In addition, the damage mechanisms of the coatings were studied during the incubation period where mass losses are negligible.

What were the most relevant findings?
The longest incubation period (271 s) was found for the thinner coating (380 µm). The highest erosion rate (2822 mg/min) was found for the thicker coating. The analysis of wear mechanisms showed formation of crazing and coalescence of cracks at the surface of the coatings during the incubation period.

What do these findings contribute?
The findings are useful to estimate the life of epoxy coatings when they are applied onto hydraulic components. In addition, the erosion rates and incubation period can be used to take decisions about thickness.

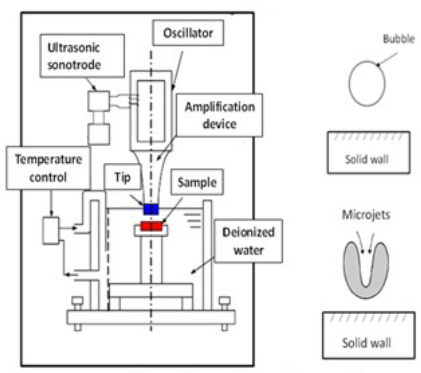

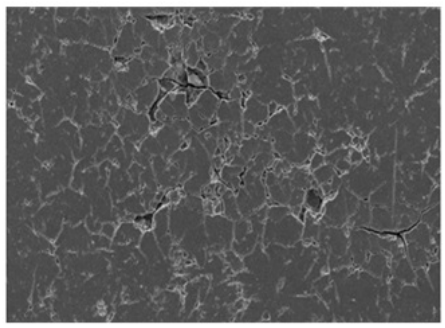

Cavitation Erosion

Wear rates and erosion mechanisms

doi: 10.25100/iyc.v27i3.14715

Introduction

Cavitation is a complex phenomenon related to the formation of bubbles of vapor and/or clusters of bubbles (1). Bubbles grow, collapse and rebound suddenly depending on the hydrodynamic and thermodynamic conditions of the cavitating flow (2-4). During the stage of collapse, bubbles may generate high temperatures and the presence of shock waves affects the surface and cause cavitation erosion (5-6).

Many studies on cavitation damage have been published but most of them are concentrated in metals and some ceramics (7-13). However, there is a growing interest in cavitation behavior under laboratory conditions of some engineering polymers (14-17), with potential application to repair hydraulic systems. However, further investigations are required to correlate damage with cavitation parameters and mechanical properties, since the results obtained by different researchers by modeling and experimental tests, show significant variations in the results (6,18-24). In the past 20 years, computational tools have been used to provide a deeper understanding of cavitation, but many physical phenomena arising during the collapse phase of bubble clusters are still under discussion (6,20-24).

Acoustic cavitation is a physical interaction of a liquid, bubbles and/or cluster of bubbles in a field of acoustic waves leading to instabilities in fluid by tensile stresses, the formation and growth of bubbles, among other events. When the bubble population and/or clusters of bubbles are subjected to oscillation processes with pressure waves of high amplitude, nonlinear pulsations are generated provoking the formation of high velocity micro jets and concentration of pressure which causes high shear stresses at the surface (25-26). Figure 1 shows a diagram of the cavitation process, when it occurs on or near a solid surface showing the stages during collapse of bubbles.

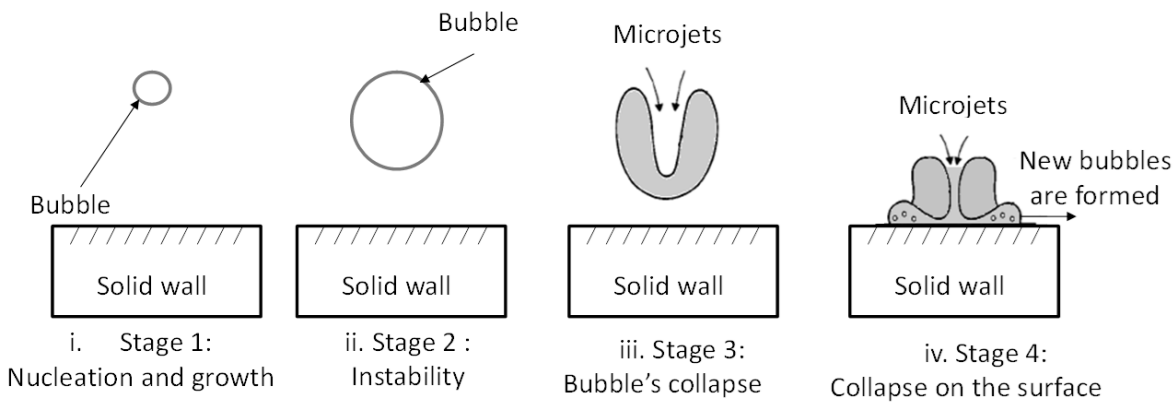

Figure. 1. Schematic representation of cavitation phenomenon which illustrates events of (i) nucleation and growth, (ii) maximum diameter and beginning of instability, (iii) collapse and microjet formation, (iv) collapse near the surface. Adapted from (2).

doi: 10.25100/iyc.v27i3.14715

During acoustic cavitation, some bubbles are formed and others grow from preexisting bubbles. This process begins in the negative portion of the acoustic cycle, when the local pressure drops below the vaporization pressure. Expansion (rarefaction) of the acoustic wave is caused by the fluid separation in sites containing the cavities. Those sites are known as weak points in the fluid. The number of bubbles forming and/or growing during the rarefaction cycle is proportional to the density of the weak points (27). Then, when the pressure of the acoustic wave is positive, the bubble's growth decreases leading to sudden collapse. This phenomenon has been previously described by Leong and his co-workers (28).

Coatings have been used to protect surfaces against cavitation erosion. Polymer coatings are interesting since they can be applied easily onto metallic surfaces. Several authors have studied the cavitation erosion of epoxy coatings (29-33). P. Veerabhadra Rao et al. (29) studied cavitation erosion of epoxy resins for concrete in water flow. They studied two epoxy resins, one with phthalic anhydride hardener, and reported the largest incubation period (60 minutes). Another important result is that P. Veerabhadra Rao et al., studied the mechanisms at the end of the tests and found that the most usual type of fracture was brittle mode. They also found that epoxy resins hardened with amine were more resistant to cavitation and observed marks that they called "melted" appearance. However, they did not study the mechanism leading to brittle fracture.

J. Zhang et al. (30) studied the resistance of non-metallic coatings to silt abrasion and cavitation erosion in a rotating disk test rig. Several coatings were evaluated: unfilled and filled epoxy, copolyamide, nylon epoxy and polyurethane. The authors found that the highest cavitation erosion resistance was obtained by polyurethane coatings. When the authors tried to correlate mechanical properties with wear resistance they found that it was not possible to establish relationships because of the complexity of the process.

Chi, S., Park, J., & Shon (31) also studied cavitation erosion resistance of epoxy resins used in the shipbuilding industry supplied by Kukdo chemical in South Korea. The authors studied commercial epoxy coatings (EP), glass- flake-reinforced epoxy coating (EGP), and silicone coating (SP). Silicone coatings reported relatively lower glass transition temperature and higher mechanical stability and showed better cavitation erosion resistance. The authors also concluded that cavitation erosion resistance is greater in coatings with better ductile and tough properties than in coating materials with higher strength or hardness.

More recently, C.E. Correa et al. (32) studied cavitation erosion resistance of epoxy and polyurethane coatings filled with inorganic particles. The largest incubation period was reported for epoxy coatings. The most important failure mechanism was removal of particles and formation of cracks around the fillers. Later on, the authors (33) removed the fillers from the matrix in order to evaluate if cavitation erosion was improved and the bond coating was also modified. In that article they studied the final damage stage for coating systems during incubation period. The authors studied cavitation erosion of epoxy systems, but cavitation behavior was reported in terms of crack length not mass losses. Moreover, the mechanisms were studied at the end of the incubation period not during the process and no simulation was done to study the phenomenon.

doi: 10.25100/iyc.v27i3.14715

Other authors (34) have investigated changes on the surface morphology induced by the cavitation erosion of a coatings based on cordierite with an epoxy matrix applied onto an aluminium substrate. The tests showed the formation of the small pits in the early stages of cavitation process, nevertheless, no emphasis was placed on the incubation stage.

On the other hand, Caisheng Huang, et all., (2024) (35) studied the failure mechanisms of epoxy and polyurea coatings with an intermediate epoxy mortar layer by ultrasonic cavitation tests during the initial stages of cavitation erosion. The investigation was focused at the formation of pits during cavitation process. The epoxy mortar as an intermediate layer significantly enhanced the material's cavitation resistance by improving its energy absorption capacity, while the polyurea's excellent elastic deformation capability reduced the likelihood of material detachment. Nevertheless, further research is required to understand the underlying mechanisms, such as the potential impact of the development of secondary cavitation pits on the intermediate coating on the progression of the primary cavitation pit.

In this paper, the cavitation erosion of epoxy coating systems subjected to vibratory cavitation tests, according to ASTM G32-99 standard was studied. The aim was to investigate the effect of thickness on cavitation erosion and since mechanical properties were expected to be thick-dependent, they were also studied. The impact pressure at the surface was estimated by considering the model of weak shock wave proposed by Colonius and co-workers (22-24). Additionally, correlations between damage observed at the surface, wear mechanisms and the results of simulation were proposed for the epoxy coating. Wear mechanisms were studied during the incubation period to understand the events leading to high wear rates at the end of the tests. A research hypothesis for this work is that the thickness of the coatings will have an effect on their cavitation erosion resistance. In addition, during the incubation period, there is damage in coatings even though the mass losses are negligible.

Materials and methods

Coating preparation and characterization

Multilayer polymeric coating systems were applied onto a steel plate (75 mm long x 25 mm wide x 3 mm thickness approximately). Two different types of resins were applied using the same procedure. Initially, two layers of epoxy-phenolic (EPF) resin without reinforcements were applied onto the surface of a stainless-steel substrate (ASTM A743 grade CA6NM). Stainless steel plates of type ASTM A743 CA6NM were cut with approximate dimensions of 75 mm x 25 mm x 3 mm in thickness. An initial polishing process was performed using a rotary polishing machine equipped with 180-grit circular sandpaper to progressively obtain a homogeneous surface. A second mechanical polishing process was conducted using a high-speed handheld polisher with 120-grit circular sandpaper discs to simulate the possible surface finish that an operator might manually apply to the blades of a turbine affected by cavitation and repaired by conventional electric arc welding procedures. Subsequently, the sample surfaces underwent a degreasing and cleaning process with acetone for 10 minutes using a vibratory ultrasonic device. Finally, a drying process was carried out for 2 minutes on the stainless-steel samples using dry air at a pressure of 4 bar.

doi: 10.25100/iyc.v27i3.14715

At the end of the surface preparation procedures, a surface roughness ranging from Ra = 3.5–4.3 µm was obtained, as measured by a contact profilometer. Following the surface preparation of the stainless-steel substrates, samples of the coating system were prepared with 2, 4, and 5 layers of epoxy coating, in addition to the anchoring and primer layer applied to the substrate. Surface preparation is important as it ensures adhesion through mechanical anchoring in the roughness of the surface. Additionally, cleaning and removal of surface contaminants further improve adhesion.

For the resins, the reactive components of Bisphenol-A-based epoxy resin, amido-amine viscosity agents, and aromatic polyamine family hardeners, among others, were used. Additionally, the coatings have titanium dioxide, silicon and aluminum oxide particles. The structural function of EPF resin was to improve adhesion of coating (bond coat) to the stainless-steel plate. After applying the bond coat, epoxy resin (EP) without reinforcements, was applied onto the epoxy-phenolic resin in several layers (multilayer) to obtain several coating thicknesses. The EP was used to generate chemical adhesion to the resin (EPF) and withstand cavitation.

The two resins (EPF) and (EP) were applied with a synthetic brush by a manual painting process. The average thickness obtained for the two layers of resin (EPF), ranged from 90 µm to 125 µm, approximately. In the case of the cavitation resistant resin (EP), the average thickness for every layer ranged from 130 to 160µm. Finally, the total thickness for each coating system corresponded to the sum of the thicknesses of the resins EPF and EP applied in layers from the steel substrate. The final thickness of the coatings to be tested in cavitation erosion were $380^{\pm 20}$ µm, $720^{\pm 20}$ µm and $920^{\pm 20}$ µm.

The reported thicknesses were determined based on tests in which different numbers of layers were applied. In this case, five layers of epoxy resin plus an epoxy-phenolic anchoring layer were applied to the substrate to achieve the greatest thickness (920 microns). For the coatings with thicknesses of 720 and 380 microns, four and two layers were applied, respectively, in addition to the same anchoring layer.

Microindentation tests were performed in an instrumented Zwick/Roell Z2.5 (TS1S) equipment equipped with an optical microscope and CCD camera available in Materials laboratory of Universidad Carlos III de Madrid-Spain. During the tests, the temperature was 25 ± 1ºC and relative humidity was 42 ± 2%. Measurements were performed on the surface of the coatings at a maximum load of 5 N at an indentation velocity of 1 Ns^{-1}. The time used during yielding was 10 seconds and a Vickers indenter according to DIN 50359-1 was used. In all cases, the reported results are the average of at least five different measurements. The standard deviation (σ) of the properties was also reported.

Cavitation tests

Cavitation tests were done in TELSONIC ULTRASONICS DG-2000 vibratory device (power of 2000 W) and the testing conditions were according to ASTM G32-09 standard. The experimental parameters used for all vibrational cavitation tests are listed in Table 1. Fig 2. shows a scheme of the testing set-up. The equipment had a water recirculation unit to control the temperature of the deionized water.

doi: 10.25100/iyc.v27i3.14715

Table 1. Parameters used for vibratory cavitation tests.

Cavitation parameter	Value
Distance from the tip of the sonotrode to the test specimen	1 mm
Oscillation frequency of sonotrode tip	20 kHz
Peak to peak amplitude of the tip of the sonotrode	50 µm
Sonotrode tip diameter	15.9 ± 0.05 mm
Cavitation fluid	Deionized water
Cavitation fluid temperature	25 ±1 °C
Test type	Indirect with the sample immersed

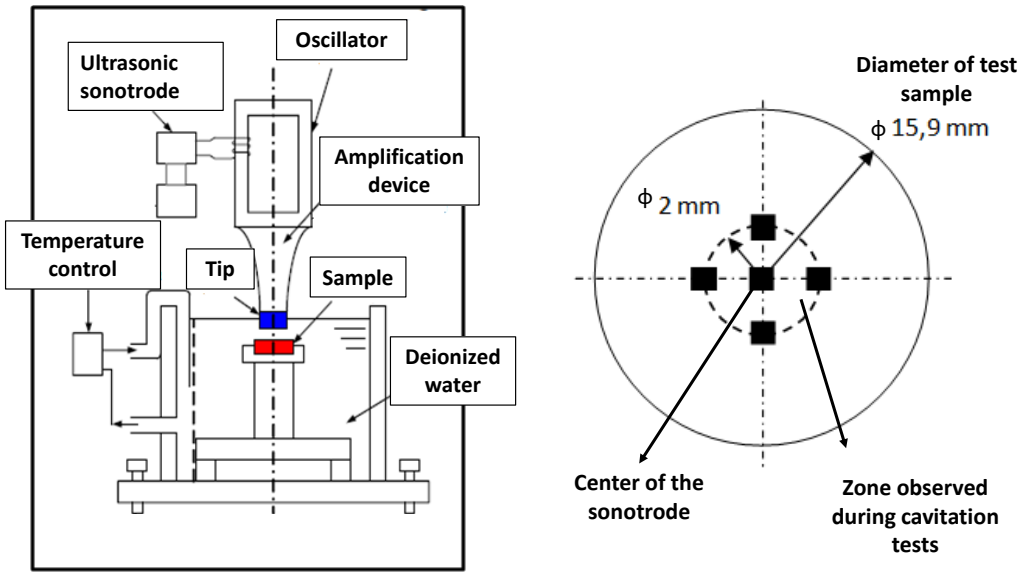

Figure 2. Scheme of the testing set-up

Test samples were ground using several emery papers (240, 320, 400, 600 and 1000 grit). In all cases, the root mean square roughness (Rq) was from 0.12 to 0.16 µm, being much lower than the value recommended in the standard (Ra=0.8 µm). Cavitation tests were done during 225 seconds and every 15 seconds test samples were removed to be observed in the SEM to evaluate the

doi: 10.25100/iyc.v27i3.14715

mechanisms of damage. The mass of samples was also measured in a scale to evaluate the erosion rate. After the tests, the incubation period was calculated for every coating. Subsequently, cavitation intervals were increased to study the cavitation behavior of the coatings, during the accelerated stage. Tests for every material were extended to evaluate wear mechanisms. At the end of cavitation tests and after every stop, samples were cleaned with deionized water, dried with dry air at 20 °C and weighted on an analytical scale with a resolution of (0.00001 g). In all cases, at least three samples were tested and the average values were reported.

Observation of cavitation surfaces

Cavitation damage was observed on a small circular central area of 2 mm of radius approximately. The selected area exhibited greater surface damage due to of the successive shock waves impacting the surface and the microjets generated during the implosion of bubble clusters. Since cavitation is randomly presented and the damage is not uniform on the surface of the test sample, the same area was selected to evaluate the evolution of damage and to evaluate the wear mechanisms for all test samples.

Tests for every material were extended to evaluate wear mechanisms. The extension of the testing periods indicates that, in order to study the mechanisms of cavitation damage, the tests were prolonged beyond the incubation period.

Estimation of Cavitation Pressures

Cavitation pressure was calculated according to the guidelines proposed by Colonius and his co-workers (22-24). In their work, they presented a systematic procedure for estimating the dynamic characteristics of the process of acoustic cavitation in bubbling flow conditions, comparable to what happens in vibratory cavitation tests. The authors are aware that the evaluation of the pressure created by the shock wave, at the vibratory cavitation, where the hydrodynamic mechanism is different from the one created by bubbling. However, in this paper the equation was used to evaluate the maximum pressure to compare it with the mechanical properties of the coatings. The acoustic wave model for weak shock is governed by the characteristic equation (1):

$$P_{\max} = \begin{cases} P_A & if \quad x < \dfrac{\pi \rho_0 c_0^3}{2\beta_0 P_A \omega} \\ \dfrac{\pi P_A}{1 + P_A\left(\dfrac{x\beta_0\omega}{\rho_0 c_0^3}\right)} & if \quad x > \dfrac{3\pi\rho_0 c_0^3}{\beta_0 P_A \omega} \end{cases} \tag{1}$$

Where: P_A is the amplitude of the acoustic pressure wave in the wall of the coating, ρ_0 and c_0 are the density and speed of sound at room temperature, ω is the frequency of oscillation of the sonotrode and β_0 is a thermodynamic nonlinearity coefficient for the bubbly cavitating flow mixture.

doi: 10.25100/iyc.v27i3.14715

The values of the parameters in the above equation to model the weak shock wave related to the oscillation amplitude P_A, the initial radius of bubble R_0, the sound velocity c in distilled water at 20°C, were taken from various references, (4,20-23,36). In all cases, the criterion used to select the values of the parameter was that researchers had demonstrated experimental validation in their analytical developments.

The conditions set for the prediction of impact pressures on the coating surface, during the vibrational cavitation test were as follows: Concentration percent of bubbles within the cluster of 1% , $(\alpha = 0.01)$; density of deionized water at 20°C, $\rho_{water} = 998 \frac{Kg}{m^3}$: polytrophic coefficient of the mixture fluid-vapor, $(\gamma = 1.4)$; sonotrode oscillation frequency, $(f = 20000\,Hz)$; the initial radius of the vapor bubble within the clusters, $(R_0 = 20\mu m)$; damping coefficient due to viscous effects in the fluid $(\delta = 0.040)$; acoustic oscillation of the bubble within the cluster, $(\omega_0 = 1.5MHz)$.Typical values of pressure drop (P_A) for water clusters were taken as 5 and 10 MPa (22).

Results and discussion

Coatings characterization

Figure 3 shows three typical cross sections of the coatings observed in the SEM. The thicknesses of the coatings were $380^{\pm 20}$ µm, $720^{\pm 20}$ µm and $920^{\pm 20}$ µm for two, four and five layers, respectively. From now on, the coatings will be named 380, 720 and 920. Resin (EPF) is mechanically attached to the surface irregularities of the steel substrate, acting as coupling layer, while the resin (EP) is chemically attached to the resin (EPF). The variation of thickness of the coatings is considered normal according to the technique used to manufacture the coatings (manual application with a brush). The coatings have titanium dioxide, silicon and aluminum oxide particles. There are minor defects at the surface such as waves and scratches caused by the manual brushing process, but they were not measured in this work. The results from EDS mapping (figure 4) showed that the coatings with $720^{\pm 20}$ µm of thickness have high contents of aluminum, silicon and titanium. The content of those elements is related to the fillers used to manufacture the coatings: aluminum and silicon oxide and titanium oxide. It must be emphasized that this work was not focused on the microstructural characteristics of the coating but in wear behavior under cavitation and the wear mechanisms. The EDS image of samples was taken before cavitation erosion tests.

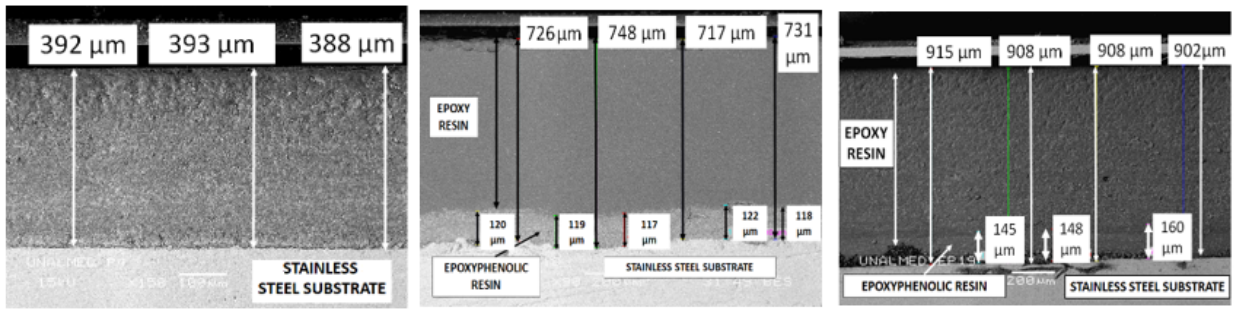

Figure. 3. Cross section of three coating systems observed in the SEM. a) Coatings with $380^{\pm 20}$ µm of thickness. b) Coatings with $720^{\pm 20}$ µm of thickness c) Coatings with $920^{\pm 20}$ µm of thickness.

doi: 10.25100/iyc.v27i3.14715

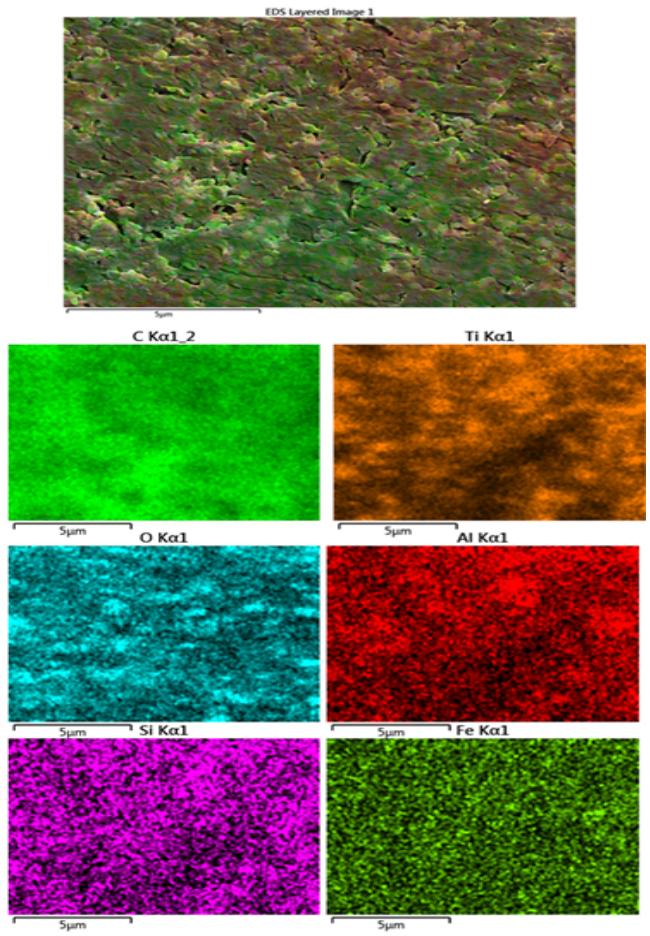

Fig. 4. EDS mapping of cross section of coatings with $720^{\pm 20}$ µm of thickness that have high contents of aluminium, silicon and titanium.

Table 2 shows a summary of the mechanical properties of the coatings. The hardness, Young´s modulus, and the yield strength are shown. The results show that the highest hardness and the largest Young´s modulus were found for the thinnest coating. The same table shows the incubation period in seconds and the maximum erosion rate (mg/min). The best behavior in terms of incubation period was found for the 380 (thinnest) coating and it also showed the lowest erosion rate. Generally speaking, the mechanical properties of 720 and 920 coatings are very similar.

doi: 10.25100/iyc.v27i3.14715

Table 2. Mechanical properties and incubation times (TI) for the coatings depending on the thickness (W). (33)

W	L	Mechanical properties (*)				Incubation period	Erosion rate*
		H	E	σ_y	H/E		
µm	**#**	**MPa**	**GPa**	**MPa**	**Adim.**	**s**	**mg/min**
$380^{\pm 20}$	2	136.00 σ=9.0%	2.800 σ=8.7%	45.33	0.0486	271	298 ±52
$720^{\pm 20}$	4	109.80 σ=5.2%	2.054 σ=2.8%	36.60	0.0535	142	312±56
$920^{\pm 20}$	5	116.00 σ=10.9%	2.130 σ=5.7%	38.66	0.0545	164	2822±423

(*): Mechanical properties obtained by instrumented micro indentation.

L: Layers of EP M: Max. erosion rate

* The error for the erosion rate was calculated by including Type A and B uncertainty

Cavitation erosion

Figure 5 shows the results of vibratory cavitation tests of coating systems. From the curve it can be concluded that there is an incubation period when the mass losses are negligible for coatings with different thicknesses. The test for the 920 coating was stopped after 225 s because the mass loss was high and the coating had severe damage. The value of the maximum erosion rate for the coatings during cavitation erosion tests (the maximum slope of the mass losses curve) is also shown in table 2. The maximum erosion rate was observed for the 920 (thickest) coating (µm). The erosion rate of the coatings with the highest erosion rate (920) was approximately nine times higher than the erosion rate for the coatings showing the best behavior (380). This result is important since the differences in erosion rates are much higher than the differences in incubation period. The differences in erosion rate can be related to the stiffness of the coatings system. The H/E ratio provides information related to the elastic strain to break and it is strongly correlated with energy dissipation in mechanical contact. When the coating is thinner the system becomes less rigid and the energy impacting the surface is dissipated through the layers of the coating and the substrate. The coating with the highest mechanical resistance and the highest Young's modulus showed the best cavitation resistance. At the end of the test, similar mass losses were observed for the 380

doi: 10.25100/iyc.v27i3.14715

coating, (15,5 mg) and the 720 coating (18,9 mg). The highest wear resistance (in terms of mass losses) was shown by the 380 coating (2 layers of EP) followed by the coating with 720 µm thickness (4 layers of EP).

The incubation period calculated from the figure was shown previously in Table 2. The longest incubation period (TI) of 271 seconds was observed for the 380 coating (2 layers of EP), whose mechanical properties (Table 2) correspond to the highest values of micro hardness (H), Young modulus (E) and yield stress (σy).

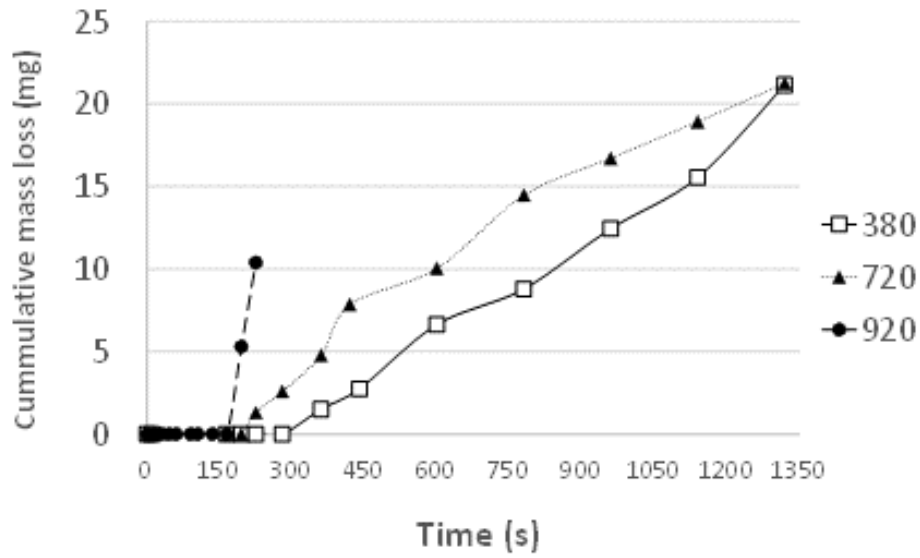

Figure. 5. Cumulative mass loss of epoxy resins after cavitation test

Cavitation Damage

Figures 6a y 6b show images of 380 and 920 coatings before cavitation tests. Figure 6c to 6e show a representative image of damage of the epoxy coating systems at the end of incubation period during cavitation erosion tests. There is evidence of plastic deformation and cracks at the surface of the coatings. Since the coatings were previously deformed by the abrasives in the emery papers, parallel lines appeared at the surface in some zones and clusters of bubbles were formed preferentially. From worn surfaces shown in Figure 5, the coating with less surface defects also reported the lowest mass losses and the lowest erosion rate (thickness 380 µm). 920 Coatings have more cracks caused by cavitation even for shorter times. These samples (920) were not evaluated up to 225 s since the damage was severe.

doi: 10.25100/iyc.v27i3.14715

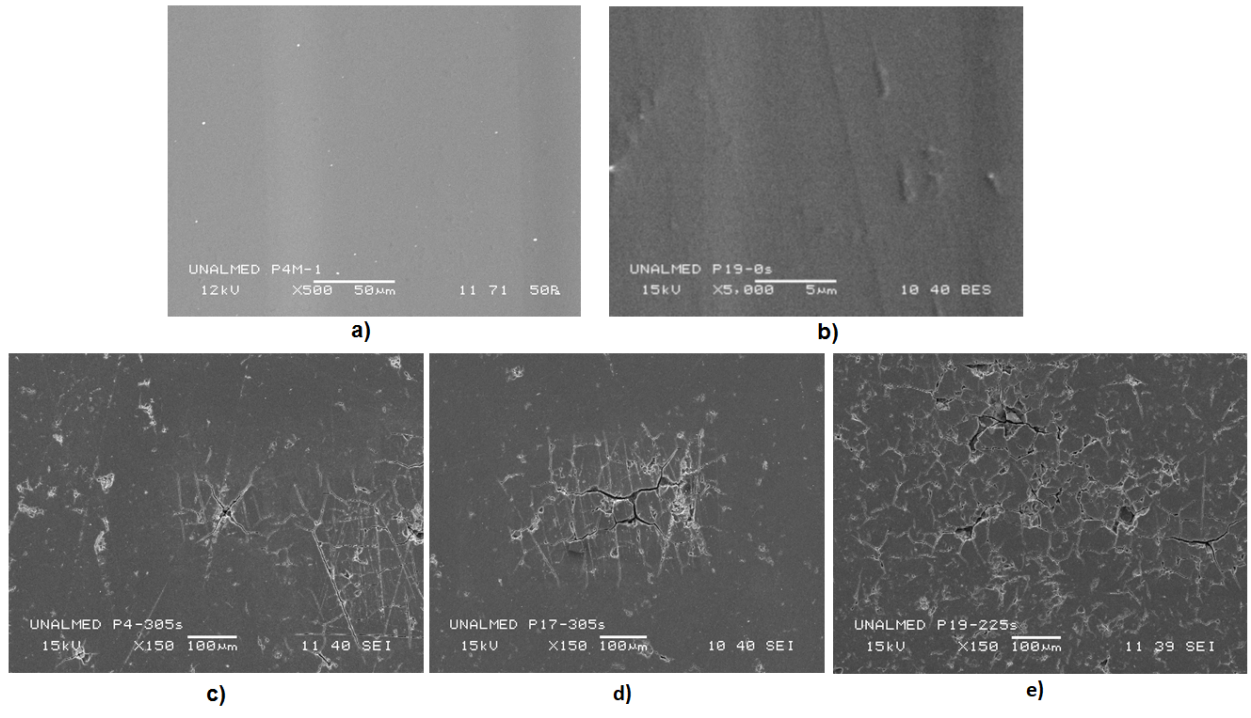

Figure. 6. Worn surfaces after cavitation for coatings with several thicknesses. Surface of the 920µm coating is the most affected by the impacts of cavitation. a) Sample 380 µm before cavitation tests b) Sample 920 µm before cavitation tests c) Coating 1: Thickness 380 µm. After 305 s d) Coating 2: Thickness 720 µm. After 305 s e) Coating 3: Thickness 920 µm. After 225 s

After the initial observation of worn surfaces of all coatings, the 720 coating was selected to characterize the damage at the surface during the tests. Figure 7 shows the cavitation damage during the test, including the incubation period, of 720 coating in the most affected area. From figure 7, cracks, caused by fatigue for all coating systems can be observed. Even though the coatings are still in the incubation period, several important mechanisms can be identified.

Initially, crazing is formed in the surface and it propagates radially around a defect of the coatings (see arrow 1 and 3 in Figure 7a). During the initial stage where crazing and crack propagation appeared, mass losses are still negligible since there is no measurable detachment of particles from the surface. Crazing appears initially in areas where the material has exhausted its capacity for deformation. Crazing can be differentiated from cracks since the former have no branches and have fibrillation between the walls (arrow 3 in figure 7a). After crazing, plastic deformation appears on the surface and new defects caused by crazing and new cracks are formed (arrows in Figure 7b).

The cracks are formed in defects and after continuous impact of bubbles, several cracks coalesce (see arrow in Figure 7c taken at the same location of Figure 7b). Moreover, plastic deformation increases in zones near the cracks since new bubbles are formed as the surface changes and becomes rougher and creates more nucleation spots. Since the bubbles collapsing near the

doi: 10.25100/iyc.v27i3.14715

surface cause surface stresses, plastic deformation under the surface is maximum (since maximum stress in surfaces under cavitation erosion are under the surface) and the cracks propagate under the surface and emerge to the surface. (see Figure 7c for details).

As the cracks coalesce, they propagate in multiple directions but radially cracks appeared preferentially (note the cracks in Figure 7d). Those cracks are caused by the shock waves. Since shock waves are bidimensional, the bubbles or clusters cause radial cracks. At the final stages when the incubation period has finished, marks appeared at the surface at a direction of grinding (see arrow 2 in Figure 7e). That result implies that the direction of polishing has a great effect since polishing causes plastic deformation at the surface and under the surfaces. At the end of the incubation period, the cumulative damage at the surface causes detachment of large particles (see arrow in Figure 7f) and mass losses start to be measurable. At the end of the incubation period, detachment of platelets caused by coalescence of cracks propagated by fatigue is extended around the surface and the maximum erosion rate is achieved.

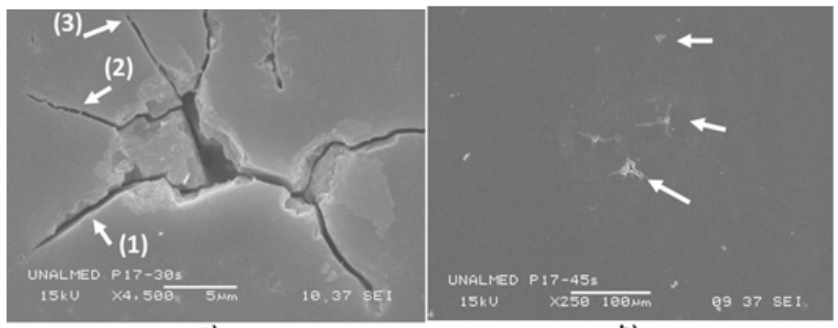

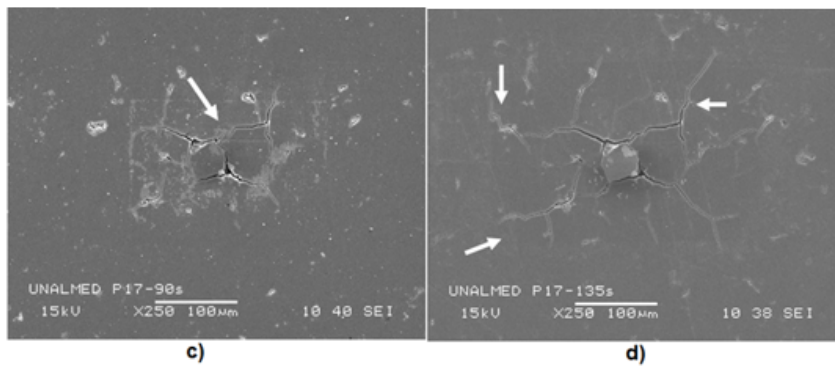

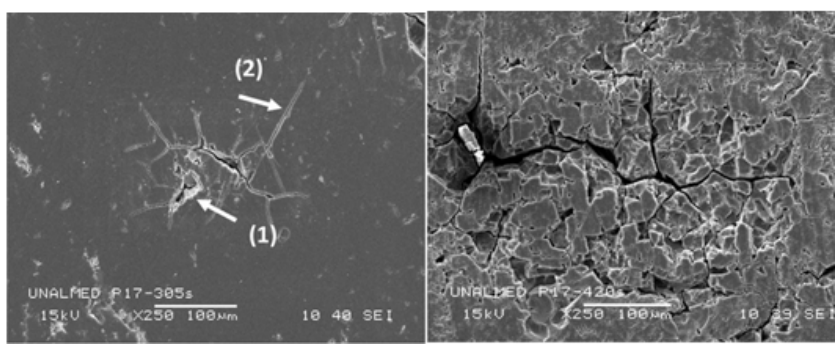

Figure. 7. Evolution of worn surfaces during cavitation tests (including the incubation period) of coating 720 a) Damage after 30 seconds b) Damage after 45 seconds c) Damage after 90 seconds d) Damage after 135 seconds e) Damage after 305 seconds f)

Damage after 420 seconds.

doi: 10.25100/iyc.v27i3.14715

Cavitation pressure

Figure 8 shows the results from the calculation at the final stages when the incubation period has finished. Marks appeared at the surface at a direction of grindingnce from the cluster to the surface wall using the weak shock model developed by Colonius and his co-workers (22). It is important to mention that cavitation bubbles near the wall also cause very high-speed micro-jets. Figures 8 a) and b) show that, when the value of the assumed acoustic pressure wave Pa (5 MPa and 10 MPa) is greater, the impact pressure of the pressure wave Pmax, at the surface of the coatings is also greater.

For the first case (Figure 8a), when PA= 5 MPa (37), the results showed that the maximum shock pressure when the cluster collapses at or near the surface with no viscous effects of fluid, is 14 MPa. However, if the collapse occurs at a distance of 100 µm from the surface, the maximum pressure decreases to 6.4 MPa. A significant reduction (equivalent to 53%) of the cluster pressure was observed. This pressure reduction is due to the viscous damping effect. For the smallest bubbles, the maximum pressure reaches values near 2 MPa.

In the second case (figure 8b), the results of the maximum pressure and its variation with the distance from the cluster to surface wall for a higher value of the acoustic pressure wave PA= 10 MPa (35) are shown. The results showed that the maximum pressure at the surface is 30 MPa. However, if the cluster collapse occurs at 100µm from the coating surface, the maximum pressure value decreases near 8 MPa, representing a significantly reduction (73%) when it is compared to the first case (figure 7a). The comparative pressure difference between the two cases, indicates that if Pmax increases, the attenuation capacity of the shock wave is also increased due to acoustic saturation effect proposed by Colonius and his co-workers (22).

Since the values of Pmax did not exceed the material yield stresses (σy), presented in Table 2 for the coatings, it could be interpreted that the damage by the impact of the shock waves and microjets causes fatigue, generated by the fluctuation of stresses varying in time and in space. These variables stresses are generated by the random collapse, rebound of bubble clusters and microjets, formed during the process of cavitation.

Even though the surfaces were shortly exposed to cavitation erosion, during that time several hundred of thousand cycles of shock waves were expected to impact the surface and cause surface fatigue. A simple calculation previously reported in the literature (36) was performed to evaluate the number of load cycles by cavitation. If a cluster of bubbles with a diameter of around 5 µm is impacting at 20 KHz the surface, during the first 15 seconds of testing the surface had been under the 300.000 cycles. Those impacts cause fatigue in the coatings observed by platelets. The mechanism of fatigue on cavitation erosion has been previously reported (14). (38)

According to Haosheng (39), growth of cracks can occur both with contact pressure over the ultimate tensile stress, and below the yield stress of the material. In the latter case, when the crack starts its propagation process, viscoelastic mechanisms are present and therefore, less energy is required for the propagation of cracks and other damage mechanisms (40).

doi: 10.25100/iyc.v27i3.14715

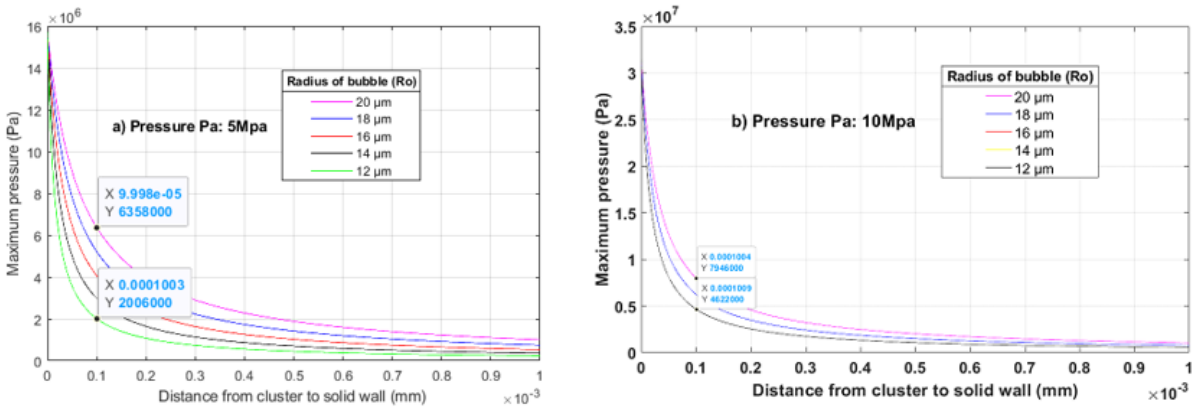

Figure. 8. Modeling results for the estimation of the pressure drop from the surface to a distance of 1 mm according to weak shock theory proposed by Colonius and his co-workers (25). a) Pressure drop obtained with Pa = 5 MPa. b) Pressure drop obtained with Pa = 10 MPa.

Conclusions

Cavitation erosion of epoxy systems with different thicknesses was studied by focusing on the mechanisms during incubation period. The most important results as described as follows:

The highest mass losses were observed for the thicker coating (920 µm) and the highest wear resistance (in terms of mass losses, erosion rate and incubation period) was shown by the coating with 380 µm thickness.

The mechanism during the incubation period is as follows: initially, crazing is formed in the surface and it propagates radially around a defect of the coatings. During the initial stages where crazing and crack propagation appeared, mass losses are still negligible since there is no measurable detachment of particles from the surface. Crazing appears initially in areas where the material has exhausted its capacity for deformation. Later, cracks appeared and they propagated radially near coating defects. During the incubation period, mass losses are still negligible since there is no measurable detachment of particles from the surface. At the end of the incubation period, cracks coalesce and detachment of particles is observed causing pits on the surface.

The maximum pressure Pmax, calculated based on the weak shock model proposed by Colonius, caused by bubbles impacting the surface did not exceed the yield stress of the multilayer epoxy coatings. Accordingly, the surface damage is attributed to fatigue processes generated by the variable, random and successive collapses of the bubble clusters. When thickness increased, defects acted as nucleation sites for cracks and wear rates were higher.

CrediT authorship contribution statement

Conceptualization - Ideas. Data Curation. Formal analysis. Investigation. Methodology: Project Management. Resources: Germán García. Software: Germán García, Albeiro Espinosa. Supervision: Germán García, Albeiro Espinosa. Validation: Germán García, Juan Felipe Santa. Writing - original

doi: 10.25100/iyc.v27i3.14715

draft - Preparation: Germán García, Juan Felipe Santa. Writing - revision and editing - Preparation: Germán García, Juan Felipe Santa, Albeiro Espinosa

Financing: does not declare. Conflict of interest: does not declare. Ethical aspect: does not declare.

References

1. Knapp RT, Dailey JW, Hammitt FG. Cavitation. New York: McGraw-Hill Book Company; 1970. Catalog Card Number 77-96428.

https://books.google.com.co/books/about/Cavitation.html?id=T-hRAAAAMAAJ&redir_esc=y

2. Brennen CE. Cavitation and bubble dynamics. Cambridge: Cambridge University Press; 2013. https://doi.org/10.1017/CBO9781107338760

3. Hammitt FG, Huang YC, Kling CL, Mitchell TM, Solomon LP. A statistically verified model for correlating volume loss due to cavitation or liquid impingement. In: Characterization and Determination of Erosion Resistance. ASTM International; 1970.

https://doi.org/10.1520/STP26875S

4. Johnsen E, Colonius T. Numerical simulations of non-spherical bubble collapse. J Fluid Mech. 2009 Jun 25;629:231. https://doi.org/10.1017/S0022112009006351

5. Shima A. Studies on bubble dynamics. Shock Waves. 1997 Feb 18;7(1):33-42.

https://doi.org/10.1007/s001930050060

6. Tomita Y. Interaction of a shock wave with a single bubble. In: Shock Wave Science and Technology Reference Library. Berlin: Springer; 2007. p. 35-66.

https://doi.org/10.1007/978-3-540-35846-6_2

7. Hattori S, Ishikura R, Zhang Q. Construction of database on cavitation erosion and analyses of carbon steel data. Wear. 2004 Nov 1;257(9-10):1022-9. https://doi.org/10.1016/j.wear.2004.07.002

8. Wenge C, Chenqing G, Kang Z, Fusan S. Correlation of cavitation erosion resistance and mechanical properties of some engineering steels. J Mater Sci. 2006 Apr 1;41(7):2151-3.

https://doi.org/10.1007/s10853-006-5209-8

9. Soyama H, Futakawa M. Estimation of incubation time of cavitation erosion for various cavitating conditions. Tribol Lett. 2004 Jul 1;17(1):27-30. https://doi.org/10.1023/B:TRIL.0000017415.79517.8c

10. Bhagat RB. Cavitation erosion of composites a materials perspective. J Mater Sci Lett. 1987 Dec 1;6(12):1473-5. https://doi.org/10.1007/BF01689327

11. Okada T, Iwai Y, Hattori S, Tanimura N. Relation between impact load and the damage produced by cavitation bubble collapse. Wear. 1995 May 1;184(2):231-9.

https://doi.org/10.1016/0043-1648(94)06581-0

12. Haosheng C, Yongjian L, Darong C, Jiadao W. Experimental and numerical investigations on development of cavitation erosion pits on solid surface. Tribol Lett. 2007 May 1;26(2):153-9.

https://doi.org/10.1007/s11249-006-9188-3

doi: 10.25100/iyc.v27i3.14715

13. Dular M, Bachert B, Stoffel B, Širok B. Relationship between cavitation structures and cavitation damage. Wear. 2004 Dec 31;257(11):1176-84. https://doi.org/10.1016/j.wear.2004.08.004

14. Hattori S, Itoh T. Cavitation erosion resistance of plastics. Wear. 2011 Jul 18;271(7):1103-8. https://doi.org/10.1016/j.wear.2011.05.012

15. Paik BG, Kim KS, Kim KY, Ahn JW, Kim TG, Kim KR, Lee SU. Test method of cavitation erosion for marine coatings with low hardness. Ocean Eng. 2011;38(13):1495-1502.

https://doi.org/10.1016/j.oceaneng.2011.07.008

16. Xu YM, Mellor BG. The effect of fillers on the wear resistance of thermoplastic polymeric coatings. Wear. 2001 Oct 31;251(1):1522-31. https://doi.org/10.1016/S0043-1648(01)00791-8

17. Böhm H, Betz S, Ball A. The wear resistance of polymers. Tribol Int. 1990 Dec 1;23(6):399-406. https://doi.org/10.1016/0301-679X(90)90055-T

18. Parlitz U, Mettin R, Luther S, Akhatov I, Voss M, Lauterborn W. Spatio-temporal dynamics of acoustic cavitation bubble clouds. Philos Trans R Soc Lond A. 1999 Feb 15;357(1751):313-34. https://doi.org/10.1098/rsta.1999.0329

19. Brennen C, Colonius T, Wang YC, Preston A. Cloud cavitation phenomena. Natl Acad Sci. 1999:239-53. https://www.researchgate.net/publication/30759127_Cloud_Cavitation_Phenomena#fullTextFileContent

20. Holzfuss J. Acoustic energy radiated by nonlinear spherical oscillations of strongly driven bubbles. Proc R Soc Lond A. 2010 Jun 8;466(2118):1829-47. https://doi.org/10.1098/rspa.2009.0594

21. Brujan EA, Ikeda T, Yoshinaka K, Matsumoto Y. The final stage of the collapse of a cloud of bubbles close to a rigid boundary. Ultrason Sonochem. 2011 Jan 31;18(1):59-64.

https://doi.org/10.1016/j.ultsonch.2010.07.004

22. Colonius T, d'Auria F, Brennen CE. Acoustic saturation in bubbly cavitating flow adjacent to an oscillating wall. Phys Fluids. 2000 Nov;12(11):2752-61. https://doi.org/10.1063/1.1313561

23. Johnson E, Colonius T, Cleveland R. Damage potential of the shock induced collapse of a gas bubble. In: Proceedings of the 7th Int Symposium on Cavitation CAV2009. Ann Arbor, 2009; CAV2009-17. https://deepblue.lib.umich.edu/items/917aad52-f903-4cd0-8de1-cbcfe023832d

24. Hilgenfeldt S, Brenner MP, Grossmann S, Lohse D. Analysis of Rayleigh-Plesset dynamics for sonoluminescing bubbles. arXiv, 1998 https://doi.org/10.1017/S0022112098001207

25. Brujan EA, Williams PR. Bubble dynamics and cavitation in non-newtonian liquids. Rheol Rev. 2005;147. https://www.researchgate.net/profile/Emil-Brujan/publication/266354042_BUBBLE_DYNAMICS_AND_CAVITATION_IN_NON-NEWTONIAN_LIQUIDS/links/5431916e0cf277d58e982b3e/BUBBLE-DYNAMICS-AND-CAVITATION-IN-NON-NEWTONIAN-LIQUIDS.pdf

26. Atchley AA, Crum LA. Acoustic Cavitation and Bubble Dynamics. University of Mississippi Physical Acoustics Research Lab; 1985 Jun 15. https://apps.dtic.mil/sti/tr/pdf/ADA156888.pdf

27. Leighton TG. What is ultrasound? Prog Biophys Mol Biol. 2007 Apr 30;93(1):3-83.

https://doi.org/10.1016/j.pbiomolbio.2006.07.026

28. Leong T, Ashokkumar M, Kentish S. The fundamentals of power ultrasound-a review. Acoust Aust. 2011 Aug 1;39(2):54-63. https://figshare.swinburne.edu.au/articles/journal_contribution/The_fundamentals_of_power_ultrasound_-_A_review/26223002?file=47528978

29. Rao PV. Evaluation of epoxy resins in flow cavitation erosion. Wear. 1988 Feb 15;122(1):77-96. https://doi.org/10.1016/0043-1648(88)90008-7

doi: 10.25100/iyc.v27i3.14715

30. Zhang J, Richardson MO, Wilcox GD, Min J, Wang X. Assessment of resistance of non-metallic coatings to silt abrasion and cavitation erosion in a rotating disk test rig. Wear. 1996 Jun 1;194(1-2):149-55. https://doi.org/10.1016/0043-1648(95)06823-6

31. Chi S, Park J, Shon M. Study on cavitation erosion resistance and surface topologies of various coating materials used in shipbuilding industry. J Ind Eng Chem. 2015 Jun 25;26:384-9.

https://doi.org/10.1016/j.jiec.2014.12.013

32. Correa CE, García GL, García AN, Bejarano W, Guzmán AA, Toro A. Wear mechanisms of epoxy-based composite coatings submitted to cavitation. Wear. 2011 Jul 29;271(9):2274-9.

https://doi.org/10.1016/j.wear.2011.01.088

33. García GL, López-Ríos V, Espinosa A, Abenojar J, Velasco F, Toro A. Cavitation resistance of epoxy-based multilayer coatings: surface damage and crack growth kinetics during the incubation stage. Wear. 2014 Aug 15;316(1):124-32. https://doi.org/10.1016/j.wear.2014.04.007

34. Pavlovic M, et al. Cavitation erosion of protective coating based on cordierite filler and epoxy matrix. Materials. 2025;18:1034. doi:10.3390/ma18051034. https://doi.org/10.3390/ma18051034

35. Huang C, et al. Cavitation pit evolution process of epoxy and polyurea coatings on mortar substrates. Ultrason Sonochem. 2024;104:106813. https://doi.org/10.1016/j.ultsonch.2024.106813

36. Wang YC, Brennen CE. Numerical computation of shock waves in a spherical cloud of cavitation bubbles. ASME J Fluids Eng. 1999;121(4):872-80. https://doi.org/10.1115/1.2823549

37. Crum LA. Acoustic cavitation. In: 1982 Ultrasonics Symposium. IEEE; 1982 Oct 27. p. 1-11. https://doi.org/10.1109/ULTSYM.1982.197778

38. Zhang YK, Hammitt FG. Cavitation erosion incubation period. Wear. 1983;86(2):299-313.

https://doi.org/10.1016/0043-1648(83)90168-0

39. Haosheng C, Shihan L. Inelastic damage by stress wave on steel surface at the incubation stage of vibration cavitation erosion. Wear. 2009 Jan 5;266(1):69-75.

https://doi.org/10.1016/j.wear.2008.05.011

40. González MG, Cabanelas JC, Baselga J. Applications of FTIR on epoxy resins-identification, monitoring the curing process, phase separation and water uptake. In: Theophilie Theopanides, editor. Infrared Spectroscopy-Materials Science, Engineering and Technology. 2012; p. 261-84. https://doi.org/10.5772/36323

doi: 10.25100/iyc.v27i3.14715